Title	Energetic Bessel-Gauss pulses from diode-pumped solid-state lasers
Author(s)	Hakola, Antti; Hakkarainen, Timo; Tommila, Rurik; Kajava, Timo
Citation	Journal of the Optical Society of America B, JOSA B vol. 27(2010):11, pp. 2342-2349
Date	2010
URL	http://dx.doi.org/10.1364/JOSAB.27.002342
Rights	Copyright © 2010 Optical Society of America. This article may be downloaded for personal use only

Energetic Bessel–Gauss pulses from diode-pumped solid-state lasers

Antti Hakola,* Timo Hakkarainen, Rurik Tommila, and Timo Kajava

Department of Applied Physics, Aalto University, P.O. Box 14100, FI-00076 AALTO, Finland

**Corresponding author: ahhakola@gmail.com*

We discuss the generation of Bessel–Gauss pulses directly from a diode-pumped solid-state laser. The laser resonator has a plano-concave configuration with the concave end mirror replaced by a diffractive phase element. As the active material, Nd-doped YLF and $GdVO_4$ crystals have been used. The pulsed operation is obtained by passively Q-switching the laser using Cr^{4+}:YAG crystals with different unsaturated transmission coefficients. When guiding the pulses out from the resonator through the laser crystal, 5–10-ns-long pulses with energies of 40–50 μJ and peak powers on the order of 10 kW are obtained. Even 70 μJ is possible but this is achieved at the expense of slightly deteriorated beam quality in the far field.

OCIS codes: 140.3295, 140.3530, 140.3540.

1. Introduction

Bessel beams have several advantages over the standard Gaussian beams in different fields of physics, biology, and engineering. The most important of these benefits are that Bessel beams retain both their width and shape upon propagation and they can be tailored to have a long and narrow focus [1, 2]. Examples of potential application areas range from precise alignment [3] and advanced three-dimensional imaging [4] to manipulating the motion of atoms and nanometer-sized particles [5–7]. With pulsed operation, also the applications where high peak powers or pulse energies are required become accessible; pulsed Bessel beams have already been utilized, e.g., in laser machining and lithographic patterning [8, 9], as pump fields in nonlinear optics [10–15], and in controlling lightning in atmosphere by means of long plasma channels [16].

Mathematically, Bessel beams can be expressed in terms of Bessel functions of different order, and they were proposed as a solution to the scalar wave equation by Durnin *et al.* [1]

in 1987. Bessel beams are immune to diffraction but, unfortunately, this also means that they are infinite by both extent and energy content. Therefore, only approximate Bessel beams can be realized in practice. One such class of approximations are Bessel–Gauss beams [17], which can be described as Bessel fields apodized by a Gaussian function e^{-r^2/w_0^2}, where w_0 is the waist radius of the beam. Due to the Gaussian part, Bessel–Gauss beams have a finite propagation-invariant range z_m which can, however, be much longer than the corresponding Rayleigh range of a Gaussian beam.

Several ways to realize Bessel–Gauss and other approximate Bessel beams have been proposed and demonstrated. The most widely used approaches are based on axicons [18–21]. Diffractive axicons, in particular, can provide almost 100-% conversion efficiency from Gaussian to Bessel-like beams when proper lithographic patterning for the axicon is applied [22]. This is, however, achieved at the expense of a challenging fabrication process and the resulting axicons tend to suffer from axial nonuniformity of the generated Bessel beam [23]. In addition, the aperture of the axicon has to be much larger than the $1/e^2$ radius of the original Gaussian beam.

As an alternative to axicons, laser resonators directly producing Bessel beams as their output have been widely studied [24–27], and several experimental realizations of such systems have been reported [28–30]. An interesting subclass of these active sources for Bessel-type beams are aspheric-mirror resonators [31]. They are able to produce exact Bessel–Gauss beams if the end mirrors are properly shaped such that the Bessel–Gauss fields are the fundamental resonant modes in the cavity. We have previously studied the generation of a zeroth-order Bessel–Gauss beam in one such resonator configuration [32]. We have used a simple linear cavity with a planar end mirror and a fully reflecting diffractive phase element as the other end mirror, and demonstrated a Nd:YAG Bessel–Gauss laser, end-pumped with a diode laser. The resulting Bessel–Gauss beams had a good quality and residual nonidealities in their intensity profiles could be explained by small fabrication errors in the surface profile of the phase element. Such ideal Bessel–Gauss beams can also be imaged by simple optical systems without deteriorating their quality [33].

The creation of pulsed Bessel beams and other Bessel pulses has been shown in a number of reports but they have mainly concentrated on the passive realization of the pulses [34–36]. Only a few approaches to create the pulses in laser resonators can be found in literature; for example, Wu *et al.* have demonstrated an axicon-based, Q-switched Nd:YAG laser able to produce Bessel–Gauss pulses with durations of 30–40 ns [37].

In this article, we discuss the production of nanosecond-long pulses from a passively Q-switched, aspheric-mirror Bessel–Gauss laser. The goal is to optimize the resonator configuration such that pulse energies up to 100 μJ become possible and that the output beam still has the desired intensity distribution. Both Nd:YLF and Nd:$GdVO_4$ have been investigated

as candidates for the laser material: $GdVO_4$ has high stimulated emission and absorption cross sections [38] whereas the long upper-state lifetime of YLF favors its use in generating pulses with a high energy and peak power [39]. Section 2 gives an overview of our approach to generate Bessel–Gauss beams. The experiments have been carried out using two different setups, described in detail in Sections 3 and 4. The obtained results are also presented in these two sections; both the continuous-wave (CW) and pulsed operation of the laser are covered. Finally, the results are summarized and conclusions are drawn in Section 5.

2. Generation of Bessel–Gauss beams in a laser resonator

In our approach, Bessel–Gauss beams and pulses are produced in a linear, plano-concave resonator with a length of d. The first cavity mirror, M1, is planar and the laser is pumped through it whereas the second one, M2, is a fully reflecting, aspheric mirror with an effective radius of curvature of $r_\mathrm{c} = 100$ mm. The role of this mirror is to alter the radial phase of the beam oscillating in the resonator in order to establish the desired Bessel–Gauss mode at wavelength λ everywhere inside the cavity. At the waist, located in the plane of the mirror M1, the field distribution of an mth order Bessel–Gauss beam in cylindrical coordinates r, ψ, and z is [31]

$$U(r, \psi, z = 0) = AJ_m(\alpha r)e^{-r^2/w_0^2}e^{im\psi}. \tag{1}$$

Here $\alpha = k \sin\theta$, $k = 2\pi/\lambda$, θ is the cone angle of the Bessel–Gauss beam, w_0 is the waist radius, J_m is the mth order Bessel function of the first kind, and A is a constant. The Fresnel propagation formula states that at a distance z the field is given by [31, 32]

$$\begin{aligned} U(r, \psi, z) &= \frac{w_0}{w(z)} \exp[\mathrm{i}\Phi(z)] e^{im\psi} J_m\left(\frac{\alpha r}{1 + \mathrm{i}z/z_\mathrm{R}}\right) \\ &\quad \times \exp\left\{-\left[\frac{1}{w^2(z)} - \frac{\mathrm{i}k}{2R(z)}\right](r^2 + \theta^2 z^2)\right\}. \end{aligned} \tag{2}$$

The parameter $\Phi(z) = kz - \alpha^2 z/(2k) - \arctan(z/z_\mathrm{R})$ stands for the axial phase, $z_\mathrm{R} = \pi w_0^2/\lambda$ is the Rayleigh range for the Gaussian envelope of the beam, and the spot size $w(z)$ and wavefront curvature $R(z)$ behave similarly to Gaussian beams.

To make the field described by Eqs. (1) and (2) a resonant mode, mirror M2 needs to be a phase-conjugating element with a complex-amplitude reflectance function of

$$t_{2,m}(r, \psi) = e^{i\phi_{2,m}(r,\psi)}, \tag{3}$$

where the phase function $\phi_{2,m}(r, \psi)$ is [31]

$$\phi_{2,m}(r, \psi) = 2\Phi(d) + 2m\psi + \frac{k\theta^2 d^2}{R(d)} + \frac{kr^2}{R(d)} + 2\arg\left[J_m\left(\frac{\alpha r}{1 + id/z_\mathrm{R}}\right)\right] \tag{4}$$

and d denotes the length of the cavity.

For our experiments, the mirror M2 was fabricated on fused silica using electron beam lithography and proportional reactive ion etching [32]. The diameter of the mirror is 2.7 mm and its high reflectivity ($R > 99\%$ at 1047–1064 nm) is obtained by depositing a 130-nm thick layer of gold on the patterned element. No damage of the coating was observed to take place at the power levels used in this work. The depth profile $h(r, \psi)$ of the element has been calculated from the relation

$$h(r, \psi) = \frac{\lambda}{2} \times \frac{\phi_{2,m}(r, \psi)}{2\pi}. \tag{5}$$

We have investigated the zeroth-order Bessel–Gauss beam ($m = 0$) at $\lambda = 1064$ nm with design parameters of $\theta = 3.75$ mrad for its cone angle and $w_0 = 300$ μm for its waist radius. These result in a propagation-invariant range of $z_0 = w_0/\theta \approx 80$ mm [32]. This particular value is shorter than the Rayleigh range of the corresponding Gaussian beam ($z_\mathrm{R} \approx 266$ mm), but with the present selection of parameters the resulting beam is a suitable compromise for demonstration purposes: it has a relatively long propagation-invariant range and shows sufficiently many intensity rings in its radial intensity profile to distinguish it from a standard Gaussian beam.

Since the Bessel–Gauss mode is created using a reflecting element, the resulting beam cannot be coupled out from the resonator through the mirror M2: the transmitted beam would be a distorted version of a zeroth-order Bessel–Gauss field. The phase-only transmission function through the element would be $\exp(i\phi_\mathrm{mod})$, where $\phi_\mathrm{mod} = kn_2H + k(n_1 - n_2)h(r, \psi)$. Here H is the thickness of the mirror M2 and n_1 and n_2 are the refractive indices of quartz and air, respectively. In this article, two alternative methods to guide the beam outside the resonator, referred to as "setup 1" and "setup 2", have been investigated. It is worth noting that both the methods provide the same Bessel–Gauss mode for the output beam: only the output coupling is different. In the first approach, an intracavity beam splitter produces another waist outside the resonator, which makes it possible to record the intensity distribution of the generated beam everywhere. The second solution relies on coupling part of the beam out from the cavity through the laser crystal, and this approach aims at maximizing the energy of the Bessel–Gauss pulses. The subsequent Sections discuss experiments with these two setups.

3. Bessel–Gauss beams and pulses using setup 1

3.A. Experiments

In the first series of experiments, a setup similar to that discussed in Refs. [32, 40] and illustrated in Fig. 1 was used. This configuration we denote as "setup 1". As the laser material, we used a 1-% Nd-doped YLF crystal (dimensions $3 \times 3 \times 5$ mm^3), whose front face (mirror M1) was coated to fully reflect the laser light at $\lambda = 1047$ nm. In addition, this face had an antireflection (AR) coating for the pump light whereas the rear face was AR coated

for 1047 nm. The other cavity mirror was the diffractive element introduced in Sec. 2. The length of the resonator could be adjusted between 38 mm and 80 mm.

The laser was end-pumped with a 4-W Unique-m.o.d.e. UM4000/100/20 pump diode operating at 798 nm. The pump beam was guided to the resonator via a multimode fiber (core diameter $d_\mathrm{f} = 100$ μm, numerical aperture $NA = 0.22$) and then collimated and focused using two positive, aspheric lenses with focal lengths of $f_1 = 4.6$ mm and $f_2 = 11.0$ mm, respectively. This resulted in a $w_\mathrm{p} \approx 120$-μm spot in the laser crystal, and we measured that 70–80% of the pump light was absorbed in the crystal. Note that the pump-beam spot in the crystal is much narrower than the mode waist radius 300 μm. The radius w_p was selected such that a good overlap between the pump beam and the $1/e^2$ width of the principal maximum of the Bessel–Gauss beam (in our case approximately 100 μm, see e.g. Fig. 2) would result. This favors the formation of a Bessel–Gauss mode instead of a Gaussian one.

The generated beam was coupled out from the laser with an intracavity glass plate. In fact four beams, reflections from the front and back faces of the plate in both forward and backward directions, were produced. To separate the beams from each other and to avoid etalon effects taking place, the glass plate was slightly wedge-shaped. Due to the optics holders and manipulators close by, the plate had to be placed at an angle of incidence of approximately $\alpha = 45^\circ \pm 10^\circ$. This angle is not too far from the Brewster angle of 56.7° so that the reflectivities of the surfaces were low, less than 2% (corresponding to $\alpha = 35^\circ$), for the linearly polarized laser mode (σ polarization). We conclude that in all our experiments with setup 1, the effective output coupling was well below 10%. The intensity profiles of the output beams and pulses were imaged with an Ophir Beamstar-Fx-50 CCD camera and the power was measured with a calorimeter.

The pulsed operation of the laser was obtained by using passively Q-switching Cr^{4+}:YAG crystals with different intial transmissions, T_0, inside the cavity. For this setup, we selected crystals with $T_0 = 41\%$, 66%, and 90%. These values have been measured at 1064 nm and at 1047 nm they are approximately 38%, 63%, and 89%, respectively [41]; in the following sections, we refer to these crystals by their nominal T_0 values. To protect the Nd:YLF crystal from excessive thermal load and avoid other thermal effects such as thermal lensing, a quasi-CW pumping scheme with 1-ms pump pulses at a repetition rate of 200 Hz was applied. The power level was also adjusted such that only a single Q-switched pulse was obtained during each pumping interval. The pulse widths were determined with the help of a fast photo detector (Thorlabs DET-100, rise time 1 ns) and a 1-GHz oscilloscope (Tektronix TDS 5104). The temporal resolution of the system is approximately 2 ns.

3.B. CW operation of setup 1

The generated CW laser beams have the desired intensity distribution of a fundamental Bessel–Gauss mode as Fig. 2 illustrates. Here both experimental and theoretical radial intensity profiles of the beam at 10 mm, 60 mm, and 380 mm from its waist are presented. In the insets one can see two-dimensional CCD images of the beam at the same distances. The cavity length was approximately 80 mm in these experiments. The theoretical profiles in Fig. 2 have been calculated from the Fresnel propagation formula of Eq. (2).

From the profiles of Fig. 2 one observes that the radial distance between the first minima is approximately 200 μm. This value remains practically intact within the whole range z_0. In the far field, the beam has transformed to a ring with a peak-to-peak diameter of 2.5 mm. These results agree perfectly with the results that we have obtained earlier from a Nd:YAG Bessel–Gauss laser [32]. The slight asymmetries in the measured profiles are caused by small fabrication errors in the surface profile of the diffractive mirror M2. These errors are also responsible for the fact that the secondary maxima and minima stay at a higher level than predicted by Eq. (2). Here one should also note that the diffractive mirror was designed for the YAG crystal with a goal depth of $\lambda/2 = 532$ nm for its surface pattern. For the YLF crystal, the goal value would be 523.5 nm, and the deviation from the actually measured average depth of 543 nm is therefore larger than 3.7%. This suggests that the functionality of the Bessel–Gauss laser is not so much dependent on the absolute value of the depth but on the proper realization of the groove profile on the mirror M2. In Ref. [32] we performed numerical simulations and they showed that a constant error in the depth profile resulted in additional losses but the beam shape remained unchanged.

The threshold pump power for the laser operation was approximately 250 mW. This value is in line with the threshold power of 265 mW for the Nd:YAG Bessel–Gauss laser. The output power increased linearly with increasing pump power and at an absorbed pump power of 1400 mW the combined power of two output beams — reflections from the back and front faces of the beam splitter — was some 230 mW.

3.C. Pulsed operation of setup 1

When inserting a Q-switching Cr^{4+}:YAG crystal in the cavity, the resulting intensity profiles within the range z_0 remain similar to the CW case. This has been illustrated in Fig. 3 (a), where the intensity profile for the output beam at 80 mm from its waist in the case of the darkest Q-switching crystal ($T_0 = 41\%$) is reproduced. In the far field, the situation is, however, significantly different: as parts (b)–(d) of Fig. 3 illustrate, an additional central peak starts to evolve as the initial transmission of the Q-switch and, simultaneously, the pulse duration decrease. These profiles have all been recorded at 380 mm from the waist using cavity lengths of 80 mm for the 90-% switch [part (b)] and 38 mm for the 66-%

and 41-% switches [parts (c) and (d)], respectively; shortening the cavity length did not have noticeable effects on the measured intensity profiles at different distances. The most probable explanation to the occurrence of the central peak is that for the shortest pulses, the number of round trips in the cavity is insufficient to form exactly the desired Bessel–Gauss mode. Another possibility is that the radial transmission of the saturable absorber changes during the pulses, which result in the central part of the Q-switching crystal to bleach earlier than the edges. This distorts the intensity profile of the pulse. The effect has been discussed in Ref. [42].

Despite the promising results for the intensity distribution, the energies of the pulses stayed at a modest level even with the darkest Q-switching crystal. With the 90-% switch in a long cavity (length 80 mm), two beams of 30-ns pulses with energies of 3 μJ were produced and shortening the cavity length to 38 mm and using the 41-% switch, resulted in 3-ns long pulses with an energy of 7.5 μJ for both output directions. The total output energy from the laser could thus be scaled only up to 15 μJ. The pulse energy is probably limited by the low output coupling. In principle, higher output couplings can be achieved by using smaller or larger angles of incidence and extra mirrors to direct the output beams past the optics holders and manipulators. However, we would still face the problem of four output beams and rather complicated alignment of the resonator, because angular adjustments of the plate laterally shift the laser mode, so that the small diffractive mirror has to be moved accordingly. For these reasons, we decided not to study the performance limits of this setup any further but switched to a more practical setup.

4. Bessel–Gauss beams and pulses using setup 2

4.A. Experiments

To scale up the pulse energy from less than 10 μJ obtained with setup 1, we changed the experimental setup of Fig. 1 to that shown in Fig. 4. This setup is called "setup 2". Now the beam was taken out from the resonator through the laser crystal and using a dichroic beam splitter inserted between the collimating and focusing lenses of the pump beam. In the actual experiments, both $GdVO_4$ and YLF crystals were used, and their front faces were coated to transmit part of the laser light at 1047 nm (for YLF) or at 1063 nm (for $GdVO_4$). Similarly to setup 1, the front faces had also an AR coating for the pump light and the back faces an AR coating for the laser light. The Nd-doping level and dimensions of the crystals as well as the reflectivity of their front faces (mirror M1) are collected in Table 1. The front face of the $GdVO_4$ crystal was also tilted by 3° from the plane orthogonal to the optical axis of the crystal. This made it possible to select one of the two polarization states for the resonant mode. In setup 2, the resonator length could be extended from 30 mm to 80 mm.

The YLF crystal was pumped with the same UM4000/100/20 diode as in setup 1 but

with a different fiber for guiding the pump beam: the core diameter was now 50 μm. As a result, the focal lengths of the collimating and focusing aspheric lenses of the pump beam differed from those mentioned in Sec. 3. The $GdVO_4$ crystal, for its part, was pumped using an Apollo Instruments S18-808-1 diode laser ($\lambda = 808.5$ nm) with powers up to 3.8 W. The parameters for the pump-beam optics as well as the approximate size of the pump beam in the laser crystal are presented in Table 2 both for the YLF and the $GdVO_4$ laser. The YLF crystal absorbed 80–90% of the pump light while the corresponding value for the $GdVO_4$ crystal was $\sim 70\%$.

For imaging the output-coupled beams with the CCD camera, an additional lens had to be inserted between the dichroic beam splitter and the camera. This way, it became possible to record the intensity distributions at all locations inside the resonator. The far-field distribution could also be studied with such a telescope system but due to geometrical restrictions the additional lenses would have to be placed relatively far away from the beam splitter and thus either large-aperture components or several successive imaging steps would have to be used. Therefore, to verify that the resonating mode in the cavity had the characteristics of a zeroth-order Bessel–Gauss beam, we visually inspected also the faint beam that leaked out from the resonator through mirror M2. At a distance $z = 380$ mm, this beam showed characteristics similar to the far-field profile obtained using setup 1. One should note that although the transmitted beam does not have the characteristics of a true Bessel–Gauss mode, in the far field the differences between these two field distributions become negligibly small. What comes to the imaged field distribution, it has been shown to behave similarly to the original beam after two lenses (focal lengths f and f') [33], although in imaging the propagation-invariant range is scaled by a factor of $(f'/f)^2$ and the waist radius by f'/f.

In setup 2, the pulsed operation was initiated using Cr^{4+}:YAG crystals with initial transmissions of 41%, 66%, 80%, and 90%. As in setup 1, a quasi-CW pumping scheme was applied for the YLF crystal but since the Apollo Instruments diode had only a continuous operation mode, the Nd:$GdVO_4$ crystal was cooled by an extra fan to better control its temperature, particularly at the highest pumping powers. For the $GdVO_4$ laser, the Tektronix oscilloscope was used to obtain both the lengths and repetition rates of the pulses. Most of the experiments were performed with the same photodiode as in setup 1 but comparison measurements were also made using an InGaAs diode (Electro-Optics Technology ET-3000), whose temporal resolution is < 1 ns.

4.B. CW operation of setup 2

Also in the case of setup 2, the intensity distributions of the output-coupled beam at different distances from the waist match well with the theoretical predictions given by Eq. (2). This is demonstrated in Figs. 5 and 6 where measured profiles at different locations for both the

$GdVO_4$ and the YLF laser are shown. For Fig. 5, the $GdVO_4$ laser has been used and the measured intensity profiles correspond to the radial profiles of the laser beam at 10 mm and 60 mm from the waist inside the resonator. Figure 6 shows a corresponding intensity profile for the beam at 40 mm from the waist in the case of the YLF laser. For the profiles in Fig. 5, we used an imaging system consisting of the focusing lens (focal length 11.0 mm) and another positive lens (focal length of 76.2 mm) and with a magnification of $M \approx 1$. For the YLF laser, the focal lengths of the two imaging lenses were 18.4 mm and 150 mm and this time the magnification of the system was $M \approx 5$. The cavity lengths were 70 mm for the $GdVO_4$ and 65 mm for the YLF laser. By taking the magnifications into account, one observes that the maxima and minima occur at the same radial distances r as in Fig. 2 and also that the relative intensities of the neighboring peaks are in accordance with Fig. 2.

The lasing threshold of the YLF laser was 600 mW of absorbed pump power and 1300 mW in the case of the $GdVO_4$ laser. Compared to the determined threshold power of 250 mW for setup 1, these values can be explained by the different output couplings of the laser cavity ($< 10\%$ in setup 1 and 20% for YLF in setup 2) which significantly alters the loss level of the cavity. In the case of the YLF crystal, the power of the output beam did not differ considerably from that obtained with setup 1: at an absorbed pump power of 1400 mW, we measured approximately 100 mW for setup 2 while for setup 1 the combined power of multiple output beams was some 200 mW at the same pump power. Considering the Nd:$GdVO_4$ laser, the output power only slightly exceeded 80 mW at the maximum absorbed pump power of 2500 mW. At such high power levels, the crystal had to be heavily cooled to prevent thermal effects from degrading the beam quality and the performance of the laser.

4.C. Pulsed operation of setup 2

As expected from the results obtained using setup 1, the pulsed operation of setup 2 did not have any noticeable effects on the intensity profiles of the output beam within the 80-mm propagation-invariant range. Examples of beam profiles at different distances from the waist are shown in Figs. 7 and 8. For the distributions in Fig. 7, the $GdVO_4$ laser with a 45-mm long cavity was used, and the measurements were made at 10 mm and 30 mm from the waist. For the profile at 10 mm, the initial transmission of the Q-switch was selected to $T_0 = 80\%$ whereas in the case of the profile at 30 mm, we used an absorber with $T_0 = 66\%$. The magnification was $M \approx 1$. Figure 8, for its part, shows two profiles measured at 40 mm from the waist when the pulsed operation was initiated in the YLF laser. Now the cavity length was 65 mm and the initial transmissions of the Q-switches were 90% and 66%. The magnification of the imaging system was $M \approx 8$.

The main improvement caused by changing the output coupling to that of setup 2 was that the energy of the generated pulses could be increased by almost a factor of 10. When

using Q-switches with $T_0 = 90\%$ and $T_0 = 66\%$ for the YLF laser, we obtained approximately 10-ns-long pulses with an energy of 40–50 μJ. By inserting the darkest crystal ($T_0 = 41\%$) in the cavity, the pulse energies increased to almost 70 μJ. The pulse length ranged from 5 to 10 ns and the peak power of the pulses was thus on the order of 10 kW.

In the $GdVO_4$ laser, the short upper-state lifetime (100 μs for $GdVO_4$, 480 μs for YLF) of the crystal limited the pulse energies to 2 μJ with the 80-% switch and to 2.5 μJ with the 66-% switch. In addition, thermal effects tended to deteriorate the beam quality and complicate the operation of the laser such that the laser could not be started with the darkest, 41-% switch. In this sense, $GdVO_4$ was a disappointment: based on the information in Ref. [38] about its large thermal conductivity, this crystal was expected to perform better. In fact, recent studies point to the direction that $GdVO_4$ actually has rather poor thermal properties compared to conventional Nd-doped crystals such as YAG and YVO_4 [43]. Our results support these observations.

5. Discussion and conclusions

We have experimentally studied the generation of nanosecond-long, Q-switched Bessel–Gauss pulses in a diode end-pumped solid-state laser. The laser was based on a plano-concave resonator where the concave end mirror had been replaced by a diffractive phase element. In these experiments, the propagation-invariant range of the Bessel–Gauss mode was designed to $z_0 = 80$ mm and the waist radius of the Gaussian envelope to $w_0 = 300$ μm. We have demonstrated that with the present selection of mode parameters, z_0 can be a factor of two larger than the cavity length and still produce a zeroth-order Bessel–Gauss beam as its output. This is in contrast with the case of resonators based on axicons to generate the desired Bessel–Gauss mode. In those systems, the field at the axicon has to be essentially the far field, and thus the cavity length needs to be much larger than the propagation-invariant range. Pääkkönen *et al.* [31] have concluded that when the beam parameters are properly chosen, the optimal phase function for the diffractive mirror M2 to generate Bessel–Gauss modes in the resonator does not noticeably change with decreasing cavity length.

As the active materials, we used 1-% Nd-doped YLF and 0.5-% Nd-doped $GdVO_4$ crystals, whose front faces were properly coated to act as the other cavity mirror for the laser wavelength. The YLF laser was observed to have better performance than the $GdVO_4$ laser, both in the CW and pulsed operation. This is associated with poor thermal properties of $GdVO_4$. The resulting Bessel–Gauss beam was coupled out from the resonator either with the help of an intracavity beam splitter (setup 1) or through the laser crystal (setup 2). Setup 1 was used for recording the intensity distributions of the produced beam at all distances whereas setup 2 enabled us to obtain a single output beam and in pulsed operation high pulse energies.

The output beam was measured to remain propagation invariant within the designed 80-mm range both in the case of setup 1 and setup 2. Also the CW output power from both the setups was approximately the same. The output power of the Bessel–Gauss laser was not as high as would be the power from a laser with a standard plano-concave resonator and a Gaussian resonant mode. For example, in the case of the YLF crystal, the CW power from the Bessel–Gauss laser was some 100 mW with an absorbed pump power of 1400 mW and in the case of the $GdVO_4$ crystal 80 mW at 2500 mW of absorbed pump power was achieved. The corresponding power levels for a Gaussian laser with a similar resonator configuration have in our studies been a factor of 5–10 higher. The slope efficiency of the Bessel–Gauss laser is thus poorer than that of a Gaussian laser while the threshold pump powers for the two types of lasers in the case of the YLF crystal are more or less comparable. This suggests higher losses in the Bessel-Gauss resonators, which is at least partly due to the observed constant error of 3.7% in the depth profile of the diffractive mirror as discussed in Sec. 3.B.

Also passively Q-switched operation of the Bessel–Gauss laser was achieved with both setup 1 and setup 2 but the highest pulse energies we measured with setup 2. The reason is most likely related to different output coupling as discussed in Sec. 3.A. The unsaturated transmission coefficient T_0 of the Q-switching Cr^{4+}:YAG crystal was varied from 90% to 41% in the experiments. In setup 1, the pulse energy could be increased up to 7.5 μJ when the darkest crystal was used in the shortest possible cavity ($d \approx 38$ mm). The pulse length in that case was approximately 3 ns. From setup 2, we obtained 40–50 μJ pulses with the 90-% and 66-% switches, but the energy could be scaled up to 70 μJ when the 41-% switch was applied. The pulse lengths were 5–10 ns and the peak power was of the order of 10 kW. The most energetic pulses were, however, achieved at the expense of a slightly degraded beam quality. The measured far-field patterns showed that the ring pattern became distorted and a clearly visible central peak appeared in the profile when T_0 decreased and when the pulses became shorter and more intense. Within the propagation-invariant range, however, no noticeable changes could be seen. Compared to a Q-switched Nd:YLF laser with a Gaussian resonant mode, the pulse energies of the Bessel–Gauss laser are only a factor of 2–3 smaller: we have obtained approximately 160-μJ pulses from a standard YLF laser with a Gaussian output beam when using the 41-% switch. In the CW case, as stated above, the difference between the two modes is considerably larger.

To summarize, our results show that Bessel–Gauss pulses with energies up to 50 μJ and durations less than 5 ns are possible when a properly doped and coated YLF crystal is used. The reported technique is thus an efficient way to create Q-switched laser pulses with propagation-invariant intensity distribution.

Acknowledgments

Antti Hakola thanks the School of Science and Technology of the Aalto University for a post-doctoral grant. The work of Timo Hakkarainen was supported by the Ministry of Education, Finland, under the Graduate School on Modern Optics and Photonics and by the Finnish Foundation for Technology Promotion. Henna Pietarinen, Janne Simonen, Pertti Pääkkönen, and Jari Turunen from the University of Eastern Finland are acknowledged for the design and fabrication of the diffractive cavity mirror used in the experiments.

References

1. J. Durnin, J. J. Miceli Jr., and J. H. Eberly, "Diffraction-free beams," Phys. Rev. Lett. **58**, 1499-1501 (1987).
2. A. Hakola, A. Shevchenko, S. C. Buchter, M. Kaivola, and N. V. Tabiryan, "Creation of a narrow Bessel-like laser beam using a nematic liquid crystal," J. Opt. Soc. Am. B **23**, 637-641 (2006).
3. C. Yu, M. R. Wang, A. J. Varela, and B. Chen, "High-density non-diffracting beam array for optical interconnection," Opt. Commun. **177**, 369-376 (2000).
4. R. Arimoto, C. Saloma, T. Tanaka, and S. Kawata, "Imaging properties of axicon in a scanning optical system," Appl. Opt. **31**, 6653-6657 (1992).
5. J. Arlt, T. Hitomi, and K. Dholakia, "Atom guiding along Laguerre-Gaussian and Bessel light beams," Appl. Phys. B **71**, 549-554 (2000).
6. V. Carvés-Chávez, D. McGloin, H. Melville, W. Sibbett, and K. Dholakia, "Simultaneous micromanipulation in multiple planes using a self-reconstructing light beam," Nature **419**, 145-147 (2002).
7. A. A. Ambardekar and Y. Li, "Optical levitation and manipulation of stuck particles with pulsed optical tweezers," Opt. Lett. **30**, 1797-1799 (2005).
8. Y. Matsuoka, Y. Kizuka, and T. Inoue, "The characteristics of laser micro drilling using a Bessel beam," Appl. Phys. A **84**, 423-430 (2006).
9. F. Courvoisier, P.-A. Lacourt, M. Jacquot, M. K. Bhuyan, L. Furfaro, and J. M. Dudley, "Surface nanoprocessing with nondiffracting femtosecond Bessel beams," Opt. Lett. **34**, 3163-3165 (2009).
10. T. Wulle and S. Herminghaus, "Nonlinear optics of Bessel beams," Phys. Rev. Lett. **70**, 1401-1405 (1993).
11. C. Altucci, R. Bruzzese, D. D'Antuoni, C. de Lisio, and S. Solimeno, "Harmonic generation in gases by use of Bessel–Gauss laser beams," J. Opt. Soc. Am. B **17**, 34-42 (2000).
12. V. Pasiskevicius, H. Karlsson, J. A. Tellefsen, F. Laurell, R. Butkus, A. Piskarskas, V.

Smilgevičius, and A. Stabinis, "Singly resonant optical parametric oscillator in periodically poled $KTiOPO_4$ pumped by a Bessel beam," Opt. Lett. **25**, 969-971 (2000).

13. S. Longhi, "Parametric amplification of spatiotemporal localized envelope waves," Phys. Rev. E **69**, 016606 (2004).
14. S. Orlov, A. Stabinis, V. Smilgevičius, G. Valiulis, and A. Piskarskas, "Parametric excitation of X-waves by downconversion of Bessel beams in nonlinear crystals," Opt. Lett. **32**, 68-70 (2007).
15. A. Averchi, D. Faccio, R. Berlasso, M. Kolesik, J. V. Moloney, A. Couairon, and P. Di Trapani, "Phase matching with pulsed Bessel beams for high-order harmonic generation," Phys. Rev. A **77** 021802 (2008).
16. J. Kasparian, R. Ackermann, Y.-B. André, G. Méchain, G. Méjean, B. Prade, P. Rohwetter, E. Salmon, K. Stelmaszczyk, J. Yu, A. Mysyrowicz, R. Sauerbrey, L. Wöste, and J.-P. Wolf, "Electric events synchronized with laser filaments in thunderclouds," Opt. Exp. **16**, 5757-5763 (2008).
17. F. Gori, G. Guattari, and C. Padovani, "Bessel-Gauss beams," Opt. Commun. **64**, 491-495 (1987).
18. J. H. McLeod, "The axicon: a new type of optical element," J. Opt. Soc. Am. **44**, 592-597 (1954).
19. J. H. McLeod, "Axicons and their uses," J. Opt. Soc. Am. **50**, 166-169 (1960).
20. K. B. Kuntz, B. Braverman, S. H. Youn, M. Lobino, E. M. Pessina, and A. I. Lvovsky, "Spatial and temporal characterization of a Bessel beam produced using a conical mirror," Phys. Rev. A **70**, 043802 (2009).
21. J. Turunen, A. Vasara, and A. T. Friberg, "Holographic generation of diffraction-free beams," Appl. Opt. **27**, 3959-3962 (1988).
22. A. Vasara, J. Turunen, and A. T. Friberg, "Realization of general nondiffracting beams with computer-generated holograms," J. Opt. Soc. Am. A **6**, 1748-1754 (1989).
23. M. Honkanen and J. Turunen, "Tandem systems for efficient generation of uniform-axial-intensity Bessel fields," Opt. Commun. **154**, 368-375 (1998).
24. J. K. Jabczyński, "A 'diffraction-free' resonator," Opt. Commun. **77**, 292-294 (1990).
25. J. Rogel-Salazar, G. H. C. New, and S. Chávez-Cerda, "Bessel-Gauss beam optical resonator," Opt. Commun. **190**, 117-122 (2001).
26. P. Muys and E. Vandamme, "Direct generation of Bessel beams," Appl. Opt. **41**, 6375-6379 (2002).
27. I. A. Litvin and A. Forbes, "Bessel-Gauss resonator with internal amplitude filter," Opt. Commun. **281**, 2385-2392 (2008).
28. K. Uehara and H. Kikuchi, "Generation of nearly diffraction-free laser beams," Appl. Phys. B **48**, 125-129 (1989).

29. A. Onae, T. Kurosawa, Y. Miki, and E. Sakuma, "Nearly diffraction-free CO_2 laser beam," J. Appl. Phys. **72**, 4529-4532 (1992).
30. A. N. Khilo, E. G. Katranji, and A. A. Ryzhevich, "Axicon-based Bessel resonator: analytical description and experiment," J. Opt. Soc. Am. A **18**, 1986-1992 (2001).
31. P. Pääkkönen and J. Turunen, "Resonators with Bessel-Gauss modes," Opt. Commun. **156**, 359-366 (1998).
32. A. Hakola, S. C. Buchter, T. Kajava, H. Elfström, J. Simonen, P. Pääkkönen, and J. Turunen, "Bessel-Gauss output beam from a diode-pumped Nd:YAG laser," Opt. Commun. **238**, 335-340 (2004).
33. M. Santarsiero, "Propagation of generalized Bessel-Gauss beams through ABCD optical systems," Opt. Commun. **132**, 1-7 (1996).
34. P. Saari and K. Reivelt, "Evidence of X-shaped propagation-invariant localized light waves," Phys. Rev. Lett. **79**, 4135-4138 (1997).
35. Z. Liu and D. Fan, "Propagation of pulsed zeroth-order Bessel beams," J. Mod. Opt. **45**, 17-21 (1998).
36. M. Clerici, O. Jedrkiewicz, E. Rubino, D. Faccio, L. Tartara, V. Degiorgio, and P. Di Trapani, "Generation and amplification of pulsed Bessel beams by seeding an optical parametric amplifier," Opt. Lett. **33**, 2296-2298 (2008).
37. F. Wu, Y. Chen, and D. Guo, Appl. Opt. 46 (2007) 4943.
38. Chr. P. Wyss, W. Lüthy, H. P. Weber, V. I. Vlasov, Yu. D. Zavartsev, P. A. Studenikin, A. I. Zagumennyi, and I. A. Shcherbakov, "Performance of a diode-pumped 5 W Nd^{3+}:$GdVO_4$ microchip laser at 1.06 μm," Appl. Phys. B **68**, 659-661 (1999).
39. D. Li, Z. Ma, R. Haas, A. Schell, P. Zhu, P. Shi, and K. Du, "Diode-end-pumped double Nd:YLF slab laser with high energy, short pulse width, and diffraction-limited quality," Opt. Lett. **33**, 1708-1710 (2008).
40. A. Hakola, S. C. Buchter, T. Kajava, H. Elfström, J. Simonen, P. Pääkkönen, and J. Turunen, "CW and pulsed operation of a diode-pumped Bessel-Gauss laser," in *Proceedings of CLEO/Europe-EQEC 2005*, Europhysics Conference Abstracts **29B** (Munich, Germany, 2005), p. CA7-3-THU.
41. H. Ridderbusch and T. Graf, "Saturation of 1047- and 1064-nm absorption in Cr^{4+}:YAG crystals", IEEE J. Quantum Electron. **43**, 168-173 (2007).
42. M. Arvidsson, "Far-field timing effect with passively Q-switched lasers," Opt. Lett. **26**, 196-198 (2001).
43. J. Didierjean, F. Balembois, F. P. Druon, P. Georges, J. Petit, P. Goldner, and B. Viana, "Comparative study of Nd:$GdVO_4$ and Nd:YVO_4, and test of a composite Nd:YVO_4/YVO_4 rod using a new method of bonding," in *Advanced Solid-State Photonics*, Technical Digest (Optical Society of America, 2006), paper WB18.

Table 1. Parameters of the laser crystals used in setup 2.

Laser crystal	Doping level	Dimensions	Reflectivity of M1
Nd:YLF	1.0%	$3 \times 3 \times 5$ mm^3	80%
Nd:$GdVO_4$	0.5%	$3 \times 3 \times 3$ mm^3	97%

Table 2. Parameters for the pump-beam optics used in setup 2.[a]

Laser crystal	d_{f} (μm)	f_1 (mm)	f_2 (mm)	w_{p} (μm)
Nd:YLF	50	6.2	18.4	75
Nd:$GdVO_4$	100	4.6	11.0	120

[a] Here d_{f} is the diameter of the fiber, f_1 and f_2 are the focal lengths of the collimating and focusing lenses, respectively, and w_{p} is the spot size in the crystal.

List of Figure Captions

Fig. 1. Schematic illustration of the diode-pumped Bessel-Gauss laser in the case of setup 1. The generated beam is coupled out from the resonator with an intracavity beam splitter.

Fig. 2. Measured radial intensity profiles together with two-dimensional CCD images (left) and theoretical profiles (right) of the CW Bessel–Gauss beam at (a) 10 mm, (b) 60 mm, and (c) 380 mm from its waist. Here setup 1 (see Fig. 1) was used and Nd:YLF acted as the active material.

Fig. 3. Measured radial intensity profiles together with two-dimensional CCD images (insets) of the generated Bessel–Gauss pulses. (a) Intensity profile at 80 mm from the waist in the case of the $T_0 = 41\%$ crystal. Parts (b)–(d) show far-field patterns at 380 mm from the waist with different Cr^{4+}:YAG crystals: (b) $T_0 = 90\%$, (c) $T_0 = 66\%$, and (d) $T_0 = 41\%$.

Fig. 4. Schematic illustration of the diode-pumped Bessel-Gauss laser in the case of setup 2. The Bessel–Gauss beam comes out from the resonator through the laser crystal.

Fig. 5. Measured radial intensity profile of the generated CW Bessel–Gauss beam at (a) 10 mm and (b) 60 mm from the waist in the case of the $GdVO_4$ laser and setup 2.

Fig. 6. Measured radial intensity profile of the generated CW Bessel–Gauss beam at 40 mm from the waist in the case of the YLF laser and setup 2. Note that the magnification is $M \approx 5$.

Fig. 7. Measured radial intensity profiles of the Bessel–Gauss pulses, produced by the $GdVO_4$ laser with setup 2, at (a) 10 mm from the waist with the $T_0 = 80$-% Q-switch and at (b) 30 mm from the waist in the case of the $T_0 = 66$-% switch.

Fig. 8. Measured radial intensity profiles of the Bessel–Gauss pulses, produced by the YLF laser with setup 2, at 40 mm from the waist and with the (a) $T_0 = 90$-% and (b) $T_0 = 66$-% Q-switch. Note that the magnification is $M \approx 8$.

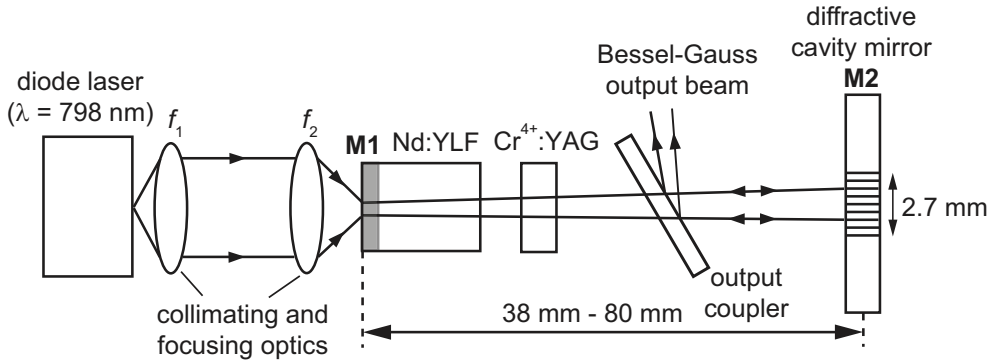

Fig. 1. Schematic illustration of the diode-pumped Bessel-Gauss laser in the case of setup 1. The generated beam is coupled out from the resonator with an intracavity beam splitter. Figure1.eps.

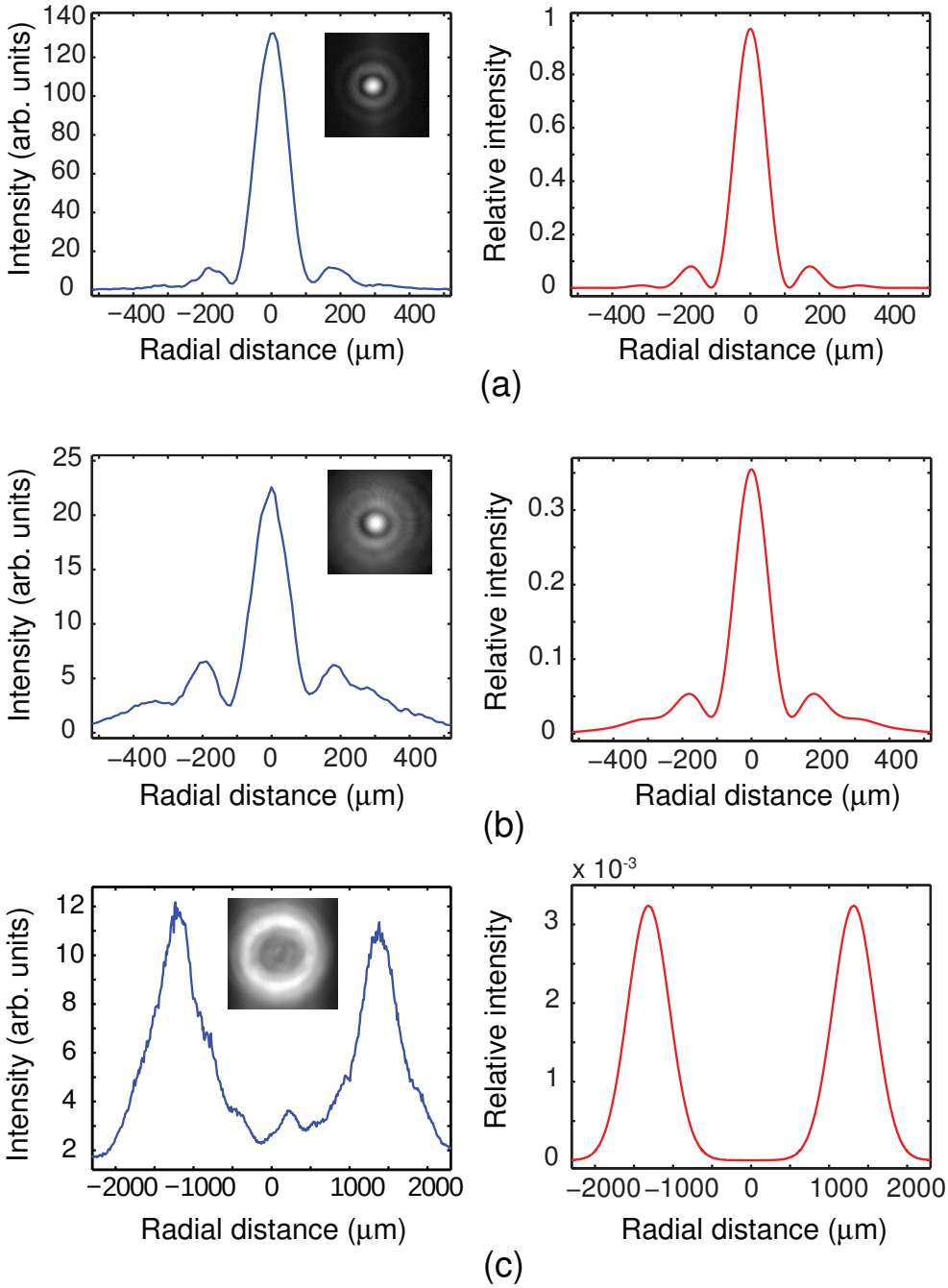

Fig. 2. Measured radial intensity profiles together with two-dimensional CCD images (left) and theoretical profiles (right) of the CW Bessel–Gauss beam at (a) 10 mm, (b) 60 mm, and (c) 380 mm from its waist. Here setup 1 (see Fig. 1) was used and Nd:YLF acted as the active material. Figure2.eps.

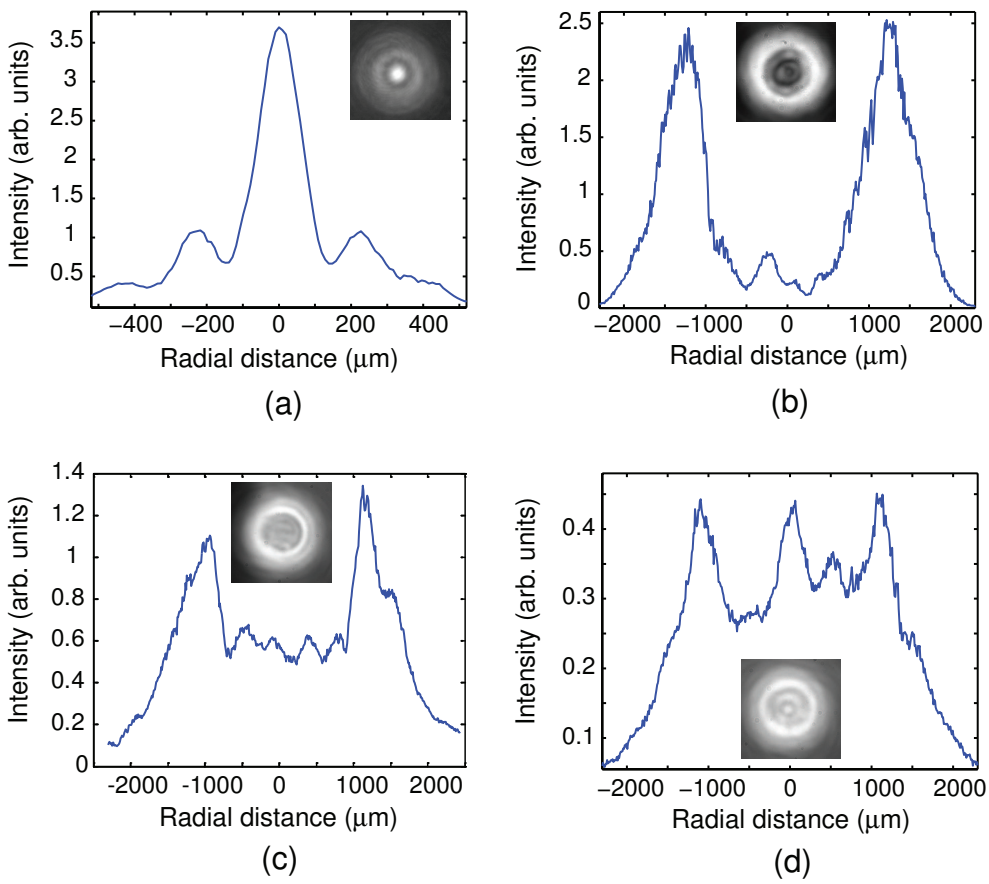

Fig. 3. Measured radial intensity profiles together with two-dimensional CCD images (insets) of the generated Bessel–Gauss pulses. (a) Intensity profile at 80 mm from the waist in the case of the $T_0 = 41\%$ crystal. Parts (b)–(d) show far-field patterns at 380 mm from the waist with different Cr^{4+}:YAG crystals: (b) $T_0 = 90\%$, (c) $T_0 = 66\%$, and (d) $T_0 = 41\%$. Figure3.eps.

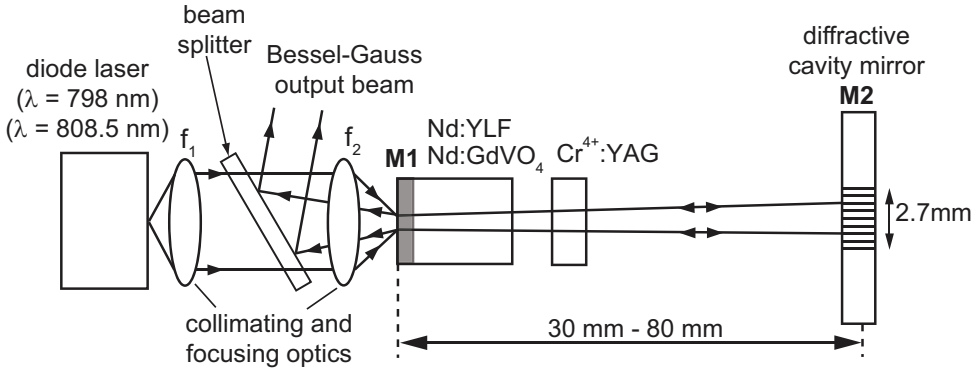

Fig. 4. Schematic illustration of the diode-pumped Bessel-Gauss laser in the case of setup 2. The Bessel–Gauss beam comes out from the resonator through the laser crystal. Figure4.eps.

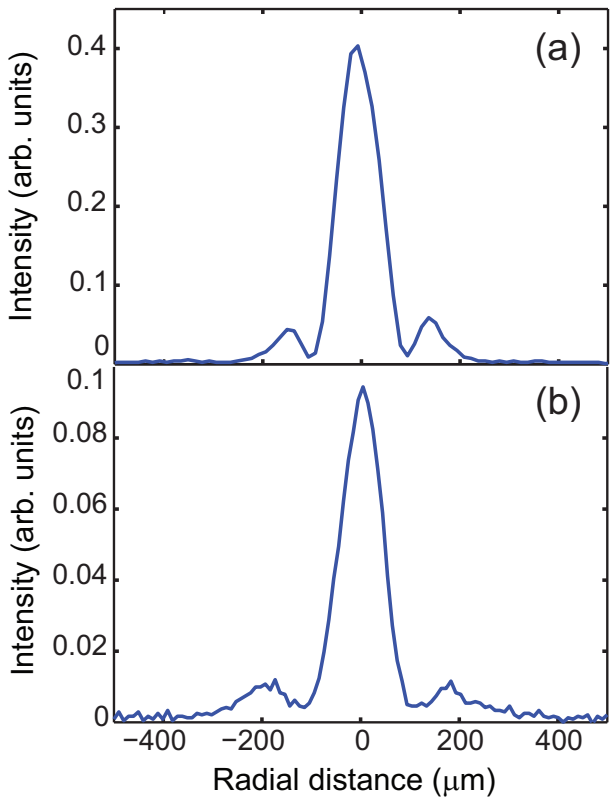

Fig. 5. Measured radial intensity profile of the generated CW Bessel–Gauss beam at (a) 10 mm and (b) 60 mm from the waist in the case of the $GdVO_4$ laser and setup 2. Figure5.eps.

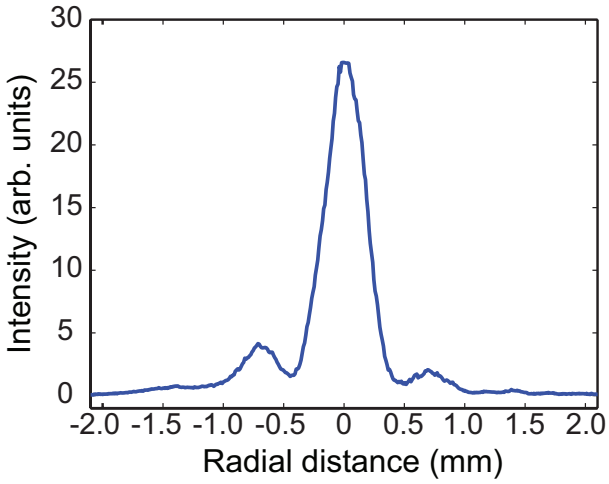

Fig. 6. Measured radial intensity profile of the generated CW Bessel–Gauss beam at 40 mm from the waist in the case of the YLF laser and setup 2. Note that the magnification is $M \approx 5$. Figure6.eps.

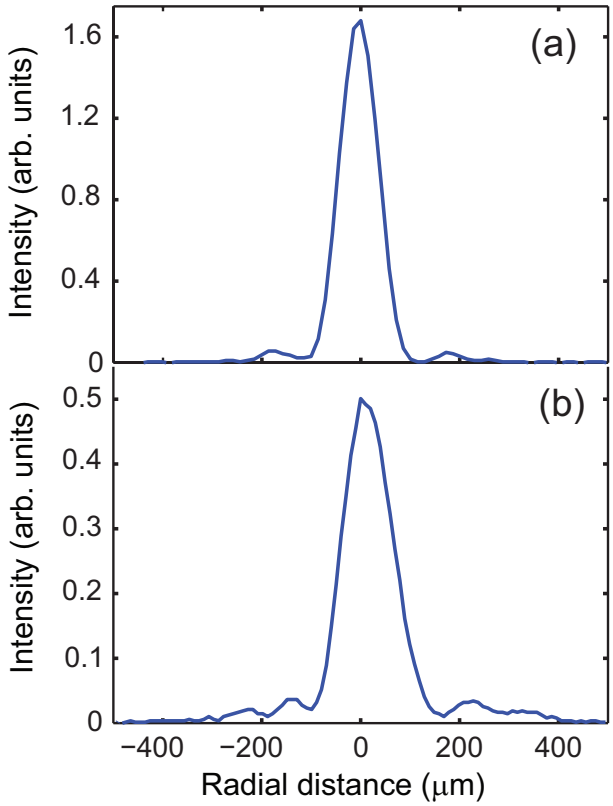

Fig. 7. Measured radial intensity profiles of the Bessel–Gauss pulses, produced by the $GdVO_4$ laser with setup 2, at (a) 10 mm from the waist with the $T_0 = 80$-% Q-switch and at (b) 30 mm from the waist in the case of the $T_0 = 66$-% switch. Figure7.eps.

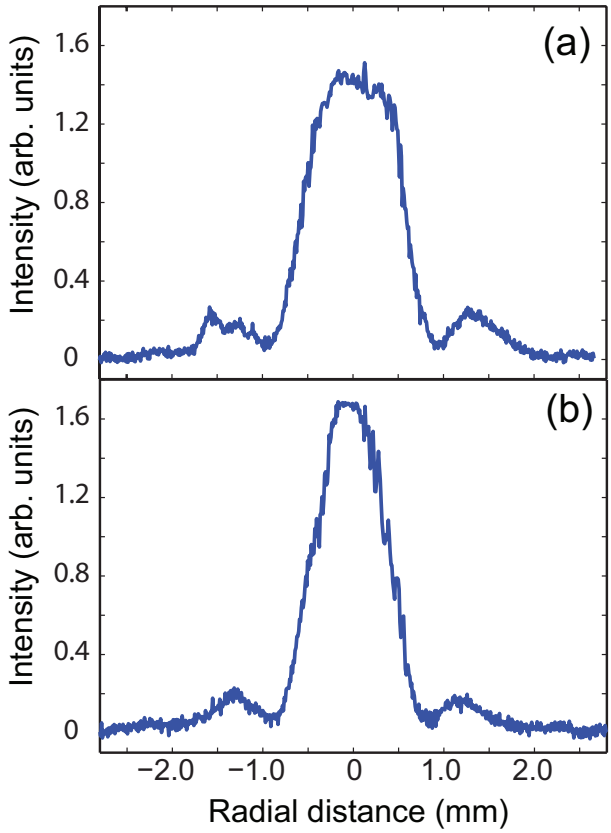

Fig. 8. Measured radial intensity profiles of the Bessel–Gauss pulses, produced by the YLF laser with setup 2, at 40 mm from the waist and with the (a) $T_0 = 90$-% and (b) $T_0 = 66$-% Q-switch. Note that the magnification is $M \approx 8$. Figure8.eps.